Grain Boundary Engineering Alloy 706 for Improved High Temperature Performance

Andrew J. Detor, Andrew D. Deal, Timothy Hanlon

General Electric Global Research Center, 1 Research Circle, Niskayuna, NY 12309

Abstract

Grain boundary engineering aims to improve material performance by optimizing the structure of interfaces in polycrystalline metals. In the present work we grain boundary engineer the Ni-Fe-based superalloy 706 and measure the effect of this process on high temperature crack growth rate. The microstructure of traditionally processed material is compared to that after grain boundary engineering using electron backscatter diffraction to identify grain boundary character according to the coincidence site lattice model. The incorporation of so called special boundaries is examined in detail through grain size and triple junction distributions. It is shown that the grain boundary engineering process can effectively disrupt the connectivity of general, crack-prone grain boundaries in the microstructure. To test a proposed structure-property relationship, crack growth rate is measured for baseline and grain boundary engineered 706 under high temperature static load – conditions which typically result in an intergranular crack path. We find an order-of-magnitude improvement in crack growth rate at low stress intensities following the grain boundary engineering process. To understand the role of grain boundary engineering in more detail we analyze secondary crack paths to determine which boundary types are truly special (i.e. arrest cracks) for this test condition. We treat the problem in a continuum way, exploring the idea that grain boundaries may become "more special" as their coincident site lattice index decreases. This approach is in contrast to the majority of the literature where a binary classification is typically assumed. The work presented here highlights the potential benefit of grain boundary engineering for improved performance of superalloys and metals in general.

Introduction

In aggressive applications involving high temperature and/or corrosive environments, preferential attack along grain boundaries can be a limiting failure mode. Metallurgists have handled this problem in a number of ways through, for example, alloy chemistry modification, coatings, or specially designed heat treatments. More recently, grain boundary engineering (GBE) has been suggested as a method to improve properties through control of grain boundary structure [1-4]. The process relies on a series of thermomechanical processes carefully designed to affect the grain boundary network in a material. It is well known that not all grain boundaries are equal; some have so called special structure where grain disorientation and boundary plane provide a low energy interface [5, 6]. The common annealing twin is a good example of a special boundary. In addition to low interfacial energy, special boundaries are also characterized by a set of beneficial properties including enhanced corrosion resistance and high creep strength [7-9]. When these boundaries are incorporated in such a way as to break up the connectivity of more susceptible general interfaces, an improvement in bulk properties can be achieved.

The most common method to classify special boundaries is through the coincident site lattice (CSL) model, where a number is assigned that defines how many atomic positions would occupy the same location in space if two adjacent grains were allowed to interpenetrate across the grain boundary [10]. For example, in a $\Sigma 9$ boundary 1 out of every 9 atoms would be coincident across the interface plane. As Σ number decreases, the grain boundary is thought to become "more special" as it approaches the limit of $\Sigma 1$ (i.e. a perfect lattice). Within the CSL model, $\Sigma 29$ is typically assumed in the literature as a threshold value, where anything equal to or lower than this number is considered special. This, however, is an arbitrary limit and more work is needed to better define how special classification should be assigned. One common criticism of the CSL model is that it ignores the grain boundary plane, which has a large impact on boundary energy and properties [6, 11]. However, determining boundary plane experimentally has a number of challenges and is currently an area of intense research [12, 13]. For the present work we use straightforward electron backscatter diffraction (EBSD) methods to quantify the Σ character of grain boundaries.

Whatever method is used to classify grain boundaries, the goal of grain boundary engineering is to increase the number and optimize the location of special boundaries in a material to affect bulk properties. Details on exactly how to characterize or measure the level of special boundaries is another area of active research. At the most basic level a simple number or length fraction of specials has been proposed. However, it is recognized that this alone is unlikely to correlate directly to properties. It is not sufficient that the number of special boundaries simply be increased, but rather their location in the microstructure, and how they are connected within the entire grain boundary network, is important [14-20]. As a simple thought experiment, imagine a crack propagating along an intergranular path – unless a junction exists where the crack sees only special boundaries, it will continue to select general susceptible boundaries, circumventing any special interfaces that may exist. For this reason, the triple junction distribution has been proposed as a more appropriate metric to quantify grain boundary engineering, and ultimately link to properties [16]. To construct this distribution, triple junctions are binned according to how many special boundaries they are coordinated with (J0, J1, J2, or J3). In the simple picture outlined above, a crack would easily propagate through a J0 (no specials), be diverted by a J1, stop at a J2, and never reach a J3. The notion that a crack can be arrested at a J2 triple junction is at the heart of grain boundary engineering, and it is this junction type we would like to maximize. Of course the picture above is a simple two dimensional description of cracking; in three dimensions the entire crack plane would need to be understood with an array of triple lines at the crack front. As three dimensional characterization methods continue to evolve [21, 22] it is expected that a more complete picture will be developed. In the present work we concentrate on the 2D triple junction distribution as it is straightforward to measure and should be useful as a screening metric to determine if a GBE process is successful from a

microstructural standpoint. In addition to triple junction analysis, we also explore the effect of GBE on grain area distributions, where special boundaries are either considered or excluded in the measurement. Observing how the area distributions shift between these two analyses provides further insight on the effectiveness of GBE in disrupting the general boundary network.

Up to this point we have discussed the concept of special boundaries, and how their presence in a microstructure may be characterized. The experimental method of introducing special boundaries in a metal is somewhat less exact, and yet another area of ongoing research [11, 23-29]. The process of GBE typically involves repetitive cycles of cold work and annealing. Cold work levels should not be so high as to cause recrystallization, but should be sufficient to provide some level of retained strain in the microstructure. Following cold work, an annealing heat treatment is conducted at relatively high temperature (greater than half the melting temperature) for a short period of time (several minutes up to an hour or so). During annealing, the retained strain from cold work drives grain boundary migration and decomposition. Decomposition has been proposed as an important mechanism for the GBE process where grain boundaries split into lower energy configurations [23]. As the cold work and annealing steps progress, typically over the course of ~3-10 cycles, low energy special boundaries are continuously created and incorporated into the general grain boundary network. When done correctly, the final microstructure will contain a low energy configuration of interfaces where special boundaries effectively break up the connectivity of the previous high energy network. More work is needed to understand GBE from a detailed mechanistic perspective; however, application of the process is relatively straightforward and with the correct set of characterization tools multiple experimental cycles can be conducted to determine the optimum process for a given material.

Most work in the literature related to GBE has been focused on the discussions above; namely processing-microstructure relationships. Less effort has been directed toward measuring the effect of the process on bulk material properties. One exception is in the area of corrosion, where GBE has been investigated and commercialized. In one example, the extent of intergranular attack under stress corrosion cracking conditions in alloy 600 was decreased by an order of magnitude following GBE [2]. In this work we are mainly interested in the effect of GBE on mechanical behavior; in particular, the effect on high temperature crack growth rate in superalloys. It has been shown that crack propagation transitions to an intergranular mechanism when some alloys are subject to sustained load at high temperature [7, 30]. GBE could therefore be a suitable method to reduce or possibly eliminate cracking along grain boundaries. Bicrystal experiments have clearly demonstrated that crack propagation rates under sustained load can be orders-of-magnitude lower for special boundaries, compared to general high angle interfaces [7]. Extending this work to polycrystals, Krupp et al. [31] have grain boundary engineered alloy 718 and shown substantial reductions in crack growth rate at elevated temperature. Gabb, et al. [32, 33] have also recently shown an improvement in the properties of 718Plus following a GBE process.

In the present work, we grain boundary engineer the Ni-Fe-based superalloy 706. EBSD is used to identify boundary character according to the CSL model for baseline and engineered microstructures. Triple junction and grain area distributions are presented to quantify the impact of GBE on the grain boundary network. High temperature crack growth rate experiments are then performed to measure the effect of GBE under industrially relevant loading conditions. Following testing, the fracture surface and crack path are examined in detail to understand how special boundaries behave and which boundary types should be considered special in this case. The sequence of processing-structure-properties presented here demonstrates the benefit of GBE in improving the performance of 706.

Experimental Procedures

706 blanks for baseline measurements were obtained from an industrial forging and given a standard solution plus two-step age heat treatment (condition 'B' in reference [34]). Grain boundary engineering blanks were machined from the same forging and subject to several cycles of cold rolling and solution annealing before the standard aging heat treat. After processing, compact tension specimens were machined from the baseline and grain boundary engineered material for crack growth rate testing. All testing was conducted at elevated temperature (538°C) in a lab air environment, and crack length was monitored using standard electric potential drop methods. Specimens were initially pre-cracked at 10 Hz prior to application of a static load to reach a starting stress intensity factor, K, of ~45 MPa-m$^{1/2}$. Under constant load, K continuously increased as the crack propagated. Plots of crack growth rate (da/dt) as a function of K are used here to measure the effectiveness of GBE. Following testing, cracked specimens were characterized by EBSD to examine the crack path in relation to grain boundary character. Specimens were cross-sectioned, mounted in a conductive phenolic compound, ground, and polished. Final polishing consisted of a minimum of 24 hours on a vibratory machine using 0.05 μm colloidal silica media. EBSD was performed using an Oxford HKL Nordlys II detector with Channel 5 software on a JEOL 6610 W-filament SEM set to 15 kV. A ~2x25 mm multi-area map of each fracture surface and a second ~4x4 mm multi-area map, used for grain size analysis, were performed. For all maps, the step size was 2.5μm and the scan rate was 100 points per second. The indexing success was over 95% for each scan, disregarding mount area. In-house cleanup routines were applied to the data to reach 100% fill and minimize artifacts in the grain and triple junction analyses. Specifically, grains were detected using a flood-fill algorithm with a grain boundary tolerance of 10° misorientation. All grains detected with sizes less than 2 data points were considered potential artifacts and removed. Iterative fill passes were then applied to the map to estimate the orientations of the 5% non-indexed points for accurate triple junction detection. During a pass, a 3x3 kernel was used to examine each non-indexed point and its immediate neighbors. A non-indexed point was filled if at least 5 of its 8 nearest neighbors contained indexed data. The fill orientation was chosen as the neighbor orientation with the smallest average misorientation from the other indexed points in the kernel. This process continued until 100% fill was reached.
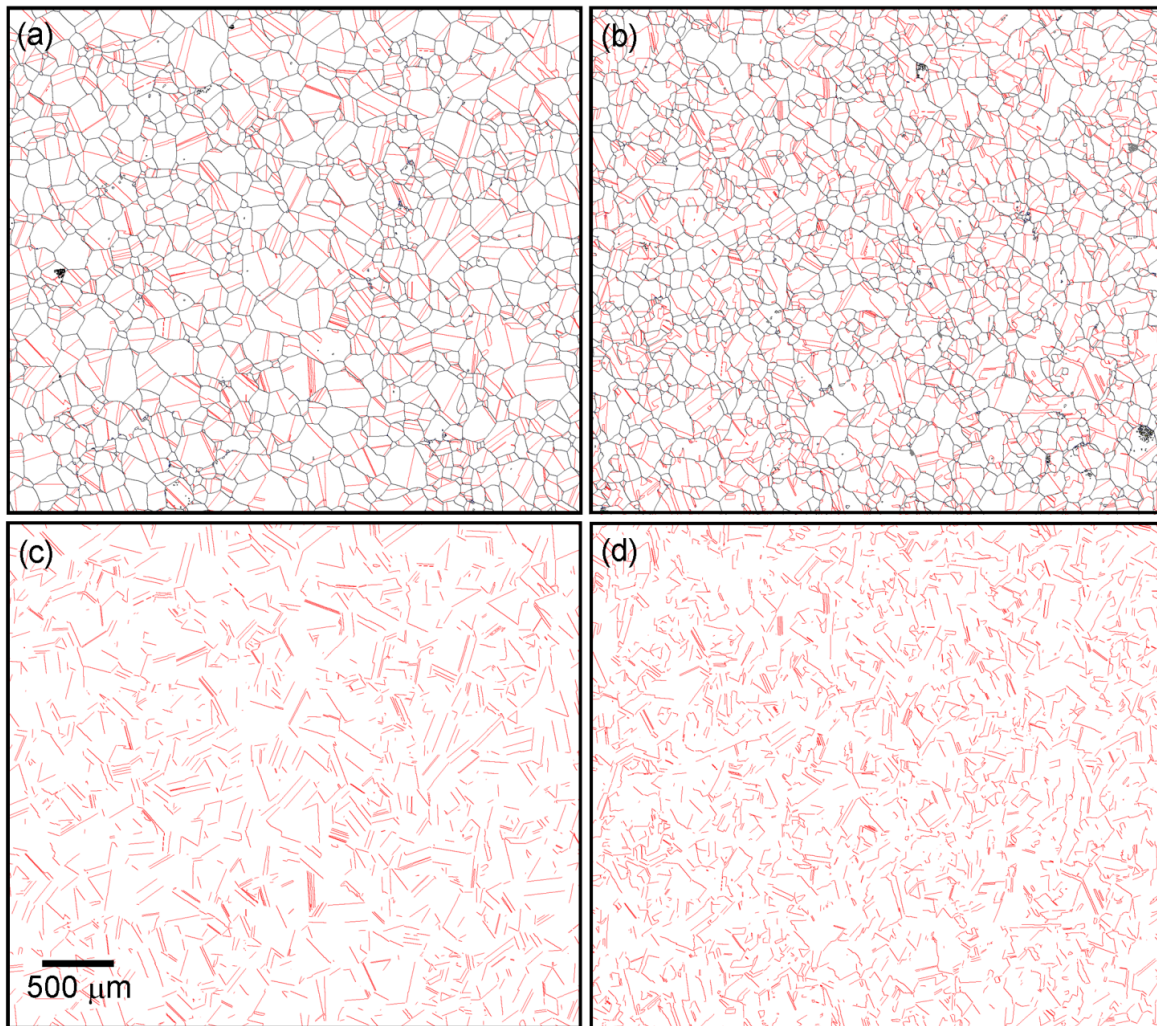
Figure 1: (a, c) Traditionally processed and (b, d) grain boundary engineered 706 microstructures. All grain boundaries are shown in (a) and (b) with coloring based on CSL index: Σ3 boundaries are red, while all other types are black. In (c) and (d), only Σ3 boundaries are displayed. Grain boundary engineering affects the nature and connectivity of Σ3 boundaries. See text for detailed discussion.

Microstructure

Baseline and grain boundary engineered 706 microstructures are presented in Fig. 1. The top two images, (a) and (b), show all boundaries for the traditionally processed and grain boundary engineered material, respectively. In these images, special boundaries are colored in red, while all other grain boundaries are black. Note that for the analysis in this section we only consider Σ3 boundaries as special. These boundaries make up the vast majority of low CSL interfaces in 706, and other face centered cubic metals in general [17]. In some cases we will comment on the effect of including the additional twin variants Σ9 and Σ27 as special; however, the frequency of these boundary types is sufficiently low that there is little effect on the outcome or conclusions. From a simple length fraction measurement, the

baseline material contains ~45% special boundaries, while that number increases to ~55% after grain boundary engineering. As discussed above, this modest increase in length fraction is not expected to be the best metric for GBE. More importantly, the nature of the special boundaries is different between the baseline and engineered microstructures. In Fig. 1(c) and (d) only special boundaries are displayed to highlight the differences. Notice that special boundaries typically cut straight across individual grains in the baseline material (c) leaving flat, isolated interfaces. These are the classic coherent Σ3 twin boundaries that normally occur in 706 and other low stacking fault energy face centered cubic metals. From a crack growth perspective, we do not expect these boundaries to have a significant impact; a crack propagating along general boundaries will never "see" these interfaces. In contrast, the grain boundary engineered structure in Fig. 1(d) contains

many special boundaries that are curved, and that intersect one another. This intersection of special boundaries is a key feature of the GBE process. Through the processing sequence, mobile special boundaries are created and interact to form J2 type triple junctions as discussed in the introduction [11, 14, 16, 23, 25, 27]. This kind of structure, where special boundaries are incorporated into the general network rather than simply bisecting individual grains, is expected to perform better in crack growth testing.

A close examination of the grain size distribution for these two materials provides more insight as to how special boundaries are incorporated into the structure. Grain area distributions are presented in Fig. 2 for the (a) baseline and (b) grain boundary
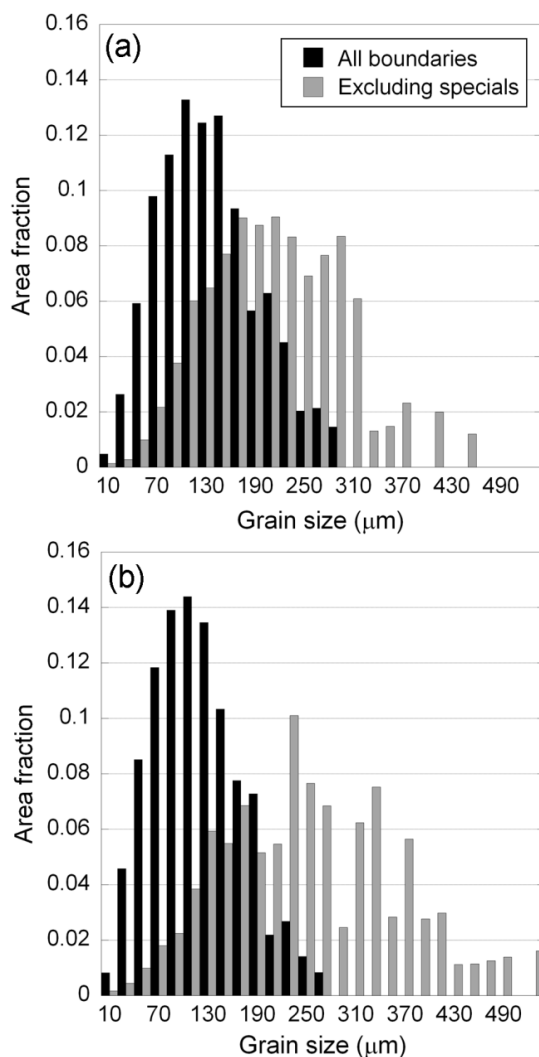

Figure 2: Grain size area distributions for (a) typical and (b) grain boundary engineered 706 showing the effect of including or excluding special boundaries from the analysis. Shifts in the mean and shape of these distributions provide insight on how special boundaries are incorporated in the microstructure. See text for details.

engineered microstructures. These distributions were constructed from the EBSD data using the Channel 5 grain detection algorithm. The general boundary tolerance was set to 10°, and Σ3 boundaries were detected using a 5° tolerance for both components of the <111>, 60° axis-angle pair description. Two cases are presented: one where *all* boundaries are considered in the analysis, and the other where special boundaries are excluded. In the baseline structure, average grain size including all boundaries is 136 μm, with a distribution that appears log-normal as expected. When special boundaries are excluded, the distribution maintains similar shape, but shifts to an average grain size of 215 μm, a factor of ~1.6 larger. Given the earlier observation that special boundaries typically cut through a single grain in the baseline structure, this shift in grain area distribution is expected. Consider the simple case where a single Σ3 boundary exactly bisects a grain; mean grain size would apparently double if that special boundary were excluded from the analysis. Turning to the grain boundary engineered structure we find a subtle, but important difference in behavior. Mean grain size including all boundaries is 119 μm, with a distribution of similar shape compare to the baseline structure. However, when special boundaries are excluded the grain area distribution does not simply shift as in the baseline case. Instead, a higher frequency of larger grains are captured in the analysis. Because special boundaries have been incorporated into the general boundary network, excluding these interfaces yields unusual grain shapes, leading to the observed shift. The average grain size in this case is 254 μm, more than a factor of 2 larger. This shift, and in particular the breakdown in log-normal character, can be used as another signature of the GBE process, showing that the general network has effectively been interrupted by special boundaries.

As discussed in the introduction, the triple junction distribution (TJD) provides a more quantitative way to determine if special
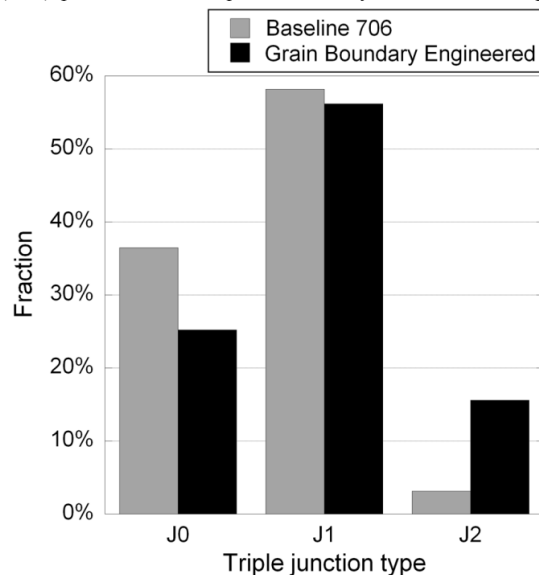

Figure 3: Triple junction distributions for traditionally processed (gray) and grain boundary engineered (black) 706. GBE results in a ~5X increase in the frequency of beneficial J2 junctions.

boundaries are incorporated into the general boundary network. To extract the TJD we use custom in-house software to locate every point in the structure were three different grains intersect. Each intersection point is then characterized as a J0, J1, J2, or J3 junction depending on the number of special boundaries it contains. Points where four grains intersect, generally artifacts of the EBSD map comprising roughly 2% of the junctions, are ignored. Distributions are presented in Fig. 3 for baseline and grain boundary engineered 706. It should be noted again that we only consider $\Sigma 3$ boundaries as special here, for reasons we will discuss in detail later on. Because of this, no J3's are shown in Fig. 3 as it is geometrically impossible to form this kind of junction [35, 36]. As previously discussed, we are looking to maximize J2 fraction through GBE under the assumption that cracks largely prefer a general grain boundary path [8]. As can be seen in Fig. 3, the J2 fraction increases from about 3% in the baseline condition to over 15% following GBE. This analysis has been repeated on at least two unique samples of baseline and grain boundary engineered materials with similar outcome. We have also run the analysis including $\Sigma 9$ and $\Sigma 27$ boundaries as special (in addition to $\Sigma 3$) and find a comparable increase in J2 fraction. The only difference in considering these extra boundary types is that J3 junctions become possible, and their fraction also increases through GBE. However, as pointed out in Refs [14, 16], we do not expect these junctions to participate in cracking, and so their increase should not affect properties as strongly as the J2 fraction. The ~5x increase in J2 junctions should translate into improved crack growth properties following the logic discussed above.

Crack Growth Rate

Up to this point we have characterized the microstructure of baseline and grain boundary engineered 706 in detail, using EBSD to quantify how special boundaries are incorporated in the general boundary network. This kind of work represents the bulk of the literature on GBE to date. Here, we extend our analysis of grain boundary engineered 706 to include a relevant property for application of this alloy: high temperature crack growth under static load. Under the testing conditions used here, cracking
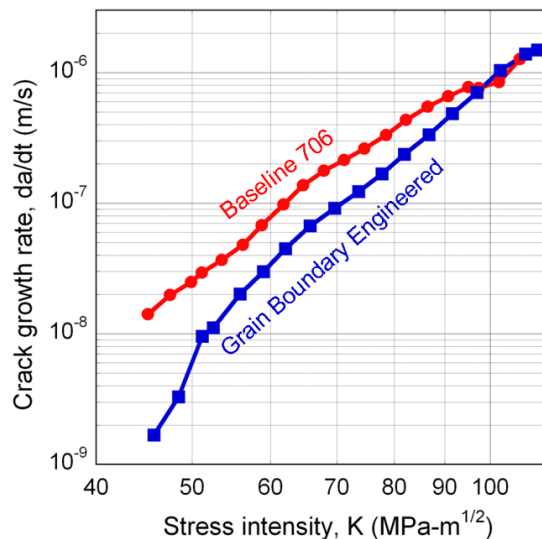

Figure 4: Static load crack growth rate as a function of stress intensity for baseline and grain boundary engineered 706 tested at 538°C. Grain boundary engineering produces an order-of-magnitude benefit at low K.

typically follows an intergranular path, making GBE an appealing process to slow crack growth rate through the introduction of special boundaries. Crack growth rate, da/dt, is plotted as a function of stress intensity, K, in Fig. 4 for baseline and engineered 706 at a test temperature of 538°C. At K values below ~90 MPa-m$^{1/2}$ the grain boundary engineered material performs better than baseline, approaching an order-of-magnitude improvement at low K. This would translate into a real benefit for component life in a damage-tolerant approach, as the initial stage of short crack growth is significantly delayed. At the highest stress intensities, above ~90 MPa-m$^{1/2}$, grain boundary
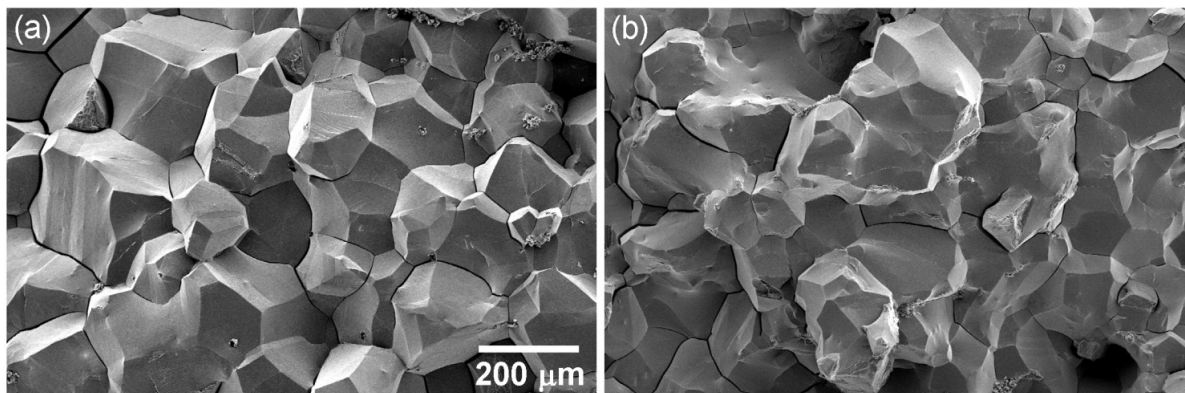

Figure 5: (a) Baseline and (b) grain boundary engineered fracture surfaces after high temperature static load crack growth testing. Both images are at the same magnification. The structure in (a) exhibits well defined intergranular cracking with clear faceting along grain boundaries; individual grains can be seen in this image. After grain boundary engineering (b), faceting around individual grains is less frequent; instead, cracking seems to occur around clusters of multiple grains. See text for more discussion on these qualitative differences.

engineering does not appear to provide any substantial benefit as crack growth rate converges with the baseline material. In this regime it is possible that an intergranular crack grows independent of grain boundary character. In other words, the driving force for crack growth may exceed a critical stress where special boundaries are no longer effective at delaying crack propagation. This idea will be explored in detail in the next section. From a practical standpoint, a part in service should never experience K values on the higher end of Fig. 4, so GBE can have an important effect on performance.

Fracture surfaces from failed compact tension specimens are shown in Fig. 5 for (a) baseline and (b) grain boundary engineered materials. These images were taken in the early stages of crack growth ($K \approx 50$ MPa-m$^{1/2}$) where GBE provides a substantial benefit. While both materials show predominately intergranular failure, close inspection reveals notable differences between the baseline and engineered structures. In the baseline condition, clear faceting along grain boundaries is observed and many individual grains can be seen on the fracture surface. This is classic intergranular failure, where each grain is isolated and acting independently. Following GBE, the fracture surface in Fig. 5(b) shows decidedly less faceting; clusters are observed where multiple grains may be acting together rather than cracking independently. This observation is consistent with expectations for a grain boundary engineered structure, where the disrupted general boundary network takes on an irregular cluster character as opposed to the well-defined traditional grain shapes in baseline material [14, 16]. Although these observations are qualitative, they help shed light on the possible mechanism leading to improved crack growth performance after GBE.

Secondary Crack Analysis

The classification of grain boundaries as general or special is a subject of considerable debate in the literature [6, 11]. As mentioned in the introduction, a rather arbitrary rule has been adopted where boundaries of $\Sigma \leq 29$ are considered special. Instead of following this kind of universal rule, we believe that special classification should be tied to a specific material, property, and operating condition of interest. For example, if intergranular corrosion resistance is required, tests should be conducted with representative material in a relevant environment to determine which boundaries are adequately resistant. This could be done through simple exposure tests, followed by cross-sectional characterization of the frontal attack coupled with EBSD. The alloy microstructure can then be optimized through GBE, focusing analysis on those special boundaries observed to perform well. In the present application, we are interested in static load crack growth in alloy 706 at 538°C. In what follows, we attempt to understand what grain boundaries are truly special under these conditions by examining secondary crack paths in correlation with grain boundary character.

Cross-sectional EBSD characterization of a failed compact tension specimen is shown in Fig. 6(a). In this image the main crack propagated from right to left and secondary cracks are observed running off the main fracture. The top image shows the general grain structure with 9 secondary cracks circled. Below this image is the corresponding EBSD map highlighting grain
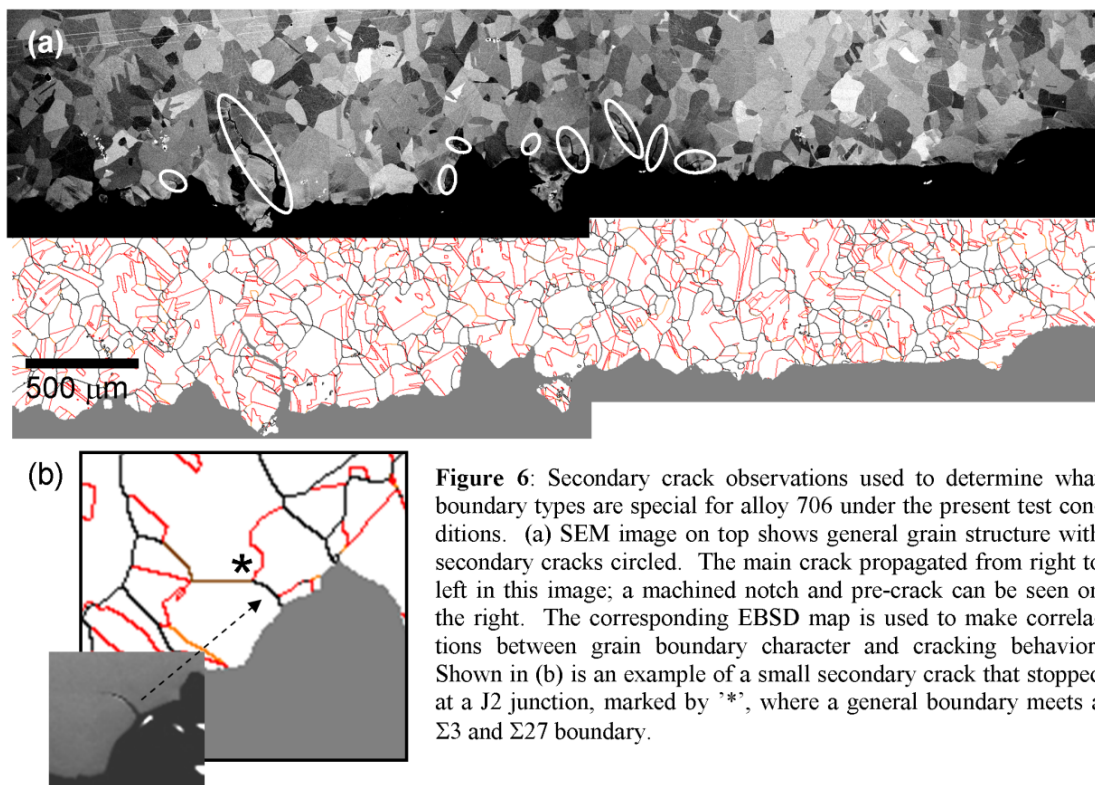

Figure 6: Secondary crack observations used to determine what boundary types are special for alloy 706 under the present test conditions. (a) SEM image on top shows general grain structure with secondary cracks circled. The main crack propagated from right to left in this image; a machined notch and pre-crack can be seen on the right. The corresponding EBSD map is used to make correlations between grain boundary character and cracking behavior. Shown in (b) is an example of a small secondary crack that stopped at a J2 junction, marked by '*', where a general boundary meets a $\Sigma 3$ and $\Sigma 27$ boundary.

boundary character (black=general boundaries, brown=Σ27, orange=Σ9, and red=Σ3). For the moment, we classify the twin variants Σ3, Σ9, and Σ27 as special. Secondary cracks allow us to observe the interaction of crack path with grain boundary character. From a simple visual inspection we find locations where cracks are arrested by J2 triple junctions as hypothesized above. For example, Fig. 6(b) shows a higher magnification view of the 6th secondary crack along the fracture in Fig. 6(a). The arrow points to a general boundary observed to fail. However, the crack did not continue beyond the J2 junction marked with a '*', which contains a Σ27 and Σ3 boundary. This is exactly the kind of behavior we expect, and a possible mechanism leading to the improved performance observed in Fig. 4.

To analyze secondary cracking in a more rigorous way we have investigated a total of 44 unique triple junctions in the grain boundary engineered and baseline samples. At each triple point the crack made a decision to either stop, or continue to propagate along one of the two neighboring boundaries. This decision is not only governed by grain boundary character, but also by the local stress intensity driving crack growth; a crack may stall simply because the adjacent boundaries lie in an unfavorable orientation with respect to the applied load, and vice-versa. To take this into account, we calculate the local mode 1 stress intensity factor along each boundary based on its orientation and position along the crack [37, 38]. To a first approximation we assume that the crack plane extends straight into the plane of the image with no inclination; as 3D reconstruction methods become more routine we can explore the local stress intensity in more detail. Under this
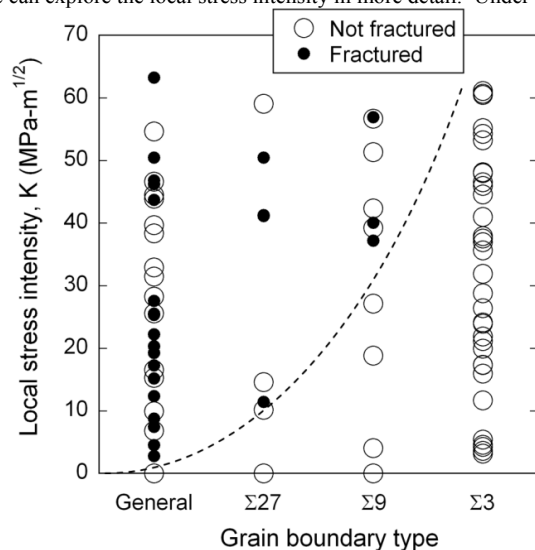

Figure 7: Grain boundary cracking map compiled from secondary crack observations. Boundaries are categorized as general, Σ27, Σ9, or Σ3. Those observed to crack are plotted as filled circles at the local stress intensity experience at that boundary, while those remaining intact are plotted as open circles. This analysis suggests that a continuum approach to grain boundary engineering should be adopted, where boundaries become more resistant to failure as their CSL index decreases.

assumption, boundaries in Fig. 6 that are perpendicular to the applied load will have higher local stress intensity than those that are nearly parallel to it. Combining grain boundary character, local stress intensity, and observations of cracking, we can begin to build an understanding of what boundaries are special for this particular test. In Fig. 7 we plot the local stress intensity vs. grain boundary character (general, Σ27, Σ9, or Σ3). In this order, grain boundaries are thought to become "more special" from left to right. The filled circles in this plot indicate boundaries that have cracked, while the open circles represent boundaries that remained intact. The most obvious outcome from this exercise is that *no* Σ3 boundaries were observed to crack, even when subject to high local stress. On the other end of the spectrum, general boundaries show mixed behavior where some crack and others do not, apparently independent of the local stress intensity. In this situation we would define a threshold stress as the lowest stress where cracking was observed – for the case of general boundaries this is ~4 MPa-m$^{1/2}$. The threshold stress for Σ3 boundaries is off the chart. In between these two extremes, the Σ27 and Σ9 interfaces show mixed behavior. Since these boundary types appear less frequently in the microstructure, fewer data points are shown in Fig. 7. Although more data is certainly needed, the information at hand suggests a possible scaling in threshold stress as indicated by the dashed line in Fig. 7, meant to serve only as a guide to the eye. Using this kind of data we can determine if and how grain boundary performance scales with Σ, and whether a continuum or binary classification is more appropriate. It is expected that future analyses in the spirit of Fig. 7 will help us better understand exactly how special each grain boundary type is for a given material and property of interest.

Summary and Conclusions

Alloy 706 was grain boundary engineered using repetitive cycles of cold work and annealing. This process increases the number of special grain boundaries in the material and, more importantly, optimizes their location within the general grain boundary network. Grain area and triple junction distributions were presented to quantitatively show the change in microstructure following GBE. In particular, the observed increase in J2 triple junctions was highlighted and discussed as a mechanism for improved material performance when failure occurs via an intergranular path. To test the effect of GBE, crack growth rate experiments were performed on baseline and engineered 706 under high temperature static load – conditions which drive intergranular failure. GBE was found to improve crack growth performance by an order of magnitude at low stress intensities. At higher stresses GBE results converge with typical baseline alloy behavior. The fracture path was investigated in detail to understand what boundary types acted as special under the present test conditions. While no Σ3 boundaries were found to fail, cracking was observed for some Σ9 and Σ27 boundaries. A strategy was outlined to analyze cracking behavior as a function of grain boundary type and local stress intensity. This method should prove useful in future studies to define what boundary types are truly special for a given application. For the present case, it appears that only Σ3 boundaries are exclusively effective at resisting intergranular cracking.

The GBE method has been studied for several decades, and is now at the point where practical application should be exploited. It is hoped that the complete processing-structure-property work

presented here will motivate future efforts to improve superalloy performance through grain boundary engineering.

References

1. Watanabe, T., Res Mechanica, 1984. **11**(1): p. 47-84.
2. Palumbo, G., E.M. Lehockey, and P. Lin, JOM, 1998. **50**(2): p. 40-43.
3. Randle, V., Mater Sci Tech, 2010. **26**(3): p. 253-261.
4. Schwartz, A.J. and W.E. King, JOM, 1998. **50**(2): p. 50-55.
5. Sutton, A.P. and R.W. Balluffi, *Interfaces in Crystalline Materials*. 1995, New York: Oxford University Press. 384-386.
6. Randle, V., Scripta Mater, 2006. **54**(6): p. 1011-1015.
7. Krupp, U., J Mat Sci, 2008. **43**(11): p. 3908-3916.
8. Kane, W.M. and C.J. McMahon Jr, Mat Sci Eng A, 2009. **507**(1-2): p. 61-65.
9. Watanabe, T., et al., Mat Sci Eng A, 2005. **410-411**: p. 140-147.
10. Grimmer, H., W. Bollmann, and D.H. Warrington, Acta Cryst A, 1974. **30**: p. 197-207.
11. Randle, V., Acta Mater, 2004. **52**(14): p. 4067-4081.
12. Saylor, D.M., et al., Metall Mater Trans A, 2004. **35 A**(7): p. 1981-1989.
13. Randle, V., et al., Acta Mater, 2008. **56**(10): p. 2363-2373.
14. Kumar, M., W.E. King, and A.J. Schwartz, Acta Mater, 2000. **48**(9): p. 2081-2091.
15. Palumbo, G., et al., Scripta Metall Mater, 1991. **25**(8): p. 1775-1780.
16. Schuh, C.A., M. Kumar, and W.E. King, Acta Mater, 2003. **51**(3): p. 687-700.
17. Schuh, C.A., M. Kumar, and W.E. King, J Mat Sci, 2005. **40**(4): p. 847-852.
18. Frary, M. and C.A. Schuh, Phys Rev B, 2004. **69**(13): p. 134115-1-134115-12.
19. Frary, M. and C.A. Schuh, Acta Mater, 2005. **53**(16): p. 4323-4335.
20. Frary, M. and C.A. Schuh, Phil Mag, 2005. **85**(11): p. 1123-1143.
21. Lewis, A.C., et al., Mat Sci Eng A, 2006. **418**(1-2): p. 11-18.
22. Uchic, M.D., et al., Ultramicroscopy, 2009. **109**(10): p. 1229-1235.
23. Kumar, M., A.J. Schwartz, and W.E. King, Acta Mater, 2002. **50**(10): p. 2599-2612.
24. Li, Q., J.R. Cahoon, and N.L. Richards, Mat Sci Eng A, 2009. **527**(1-2): p. 263-271.
25. Randle, V., Acta Mater, 1999. **47**(15): p. 4187-4196.
26. Randle, V. and M. Coleman, Acta Mater, 2009. **57**(11): p. 3410-3421.
27. Randle, V. and G. Owen, Acta Mater, 2006. **54**(7): p. 1777-1783.
28. Schwartz, A.J., W.E. King, and M. Kumar, Scripta Mater, 2006. **54**(6): p. 963-968.
29. Zhang, Y.B., et al., Mater Sci Tech, 2010. **26**(2): p. 197-202.
30. Pfaendtner, J.A. and C.J. McMahon, Acta Mater, 2001. **49**(16): p. 3369-3377.
31. Krupp, U., et al., Mat Sci Eng A, 2003. **349**(1-2): p. 213-217.
32. Gabb, T.P., et al. in *7th International Symposium on Superalloy 718 and Derivatives*. 2010. Pittsburgh, PA.
33. Lin, P., et al. in *7th International Symposium on Superalloy 718 and Derivatives*. 2010. Pittsburgh, PA.
34. *Inconel Alloy 706 Technical Datasheet*. Available from: www.specialmetals.com/products/inconelalloy706.
35. Miyazawa, K., et al., Acta Cryst A, 1996. **52**(6): p. 787-796.
36. Frary, M. and C.A. Schuh, Acta Mater, 2003. **51**(13): p. 3731-3743.
37. Cotterell, B. and J.R. Rice, Int J Fract, 1980. **16**(2): p. 155-169.
38. Suresh, S., Metall Trans A, 1985. **16**(2): p. 249-260.